SAND98-2557J

# Composition and Bonding in Amorphous Carbon Films Grown by Ion Beam Assisted Deposition: Influence of the Assistance Voltage.

R. Gago, I. Jiménez, and J. M. Albella
Instituto de Ciencia de Materiales de Madrid (CSIC), 28049 Madrid, Spain.

A. Climent-Font
Dpto. de Física Aplicada (C-XII) Univ. Autónoma de Madrid. 28049 Madrid, Spain.

L. J. Terminello
Lawrence Livermore National Laboratory, Livermore, California 94550.

J.C. Banks and B.L. Doyle
Sandia National Laboratories, Radiation Solid Interactions and Processing. Albuquerque, N.M.87185-1056, U.S.A.



## ABSTRACT

Amorphous carbon films have been grown by evaporation of graphite with concurrent $Ar^+$ ions bombardment assistance. The ion energy has been varied between 0-800 V while keeping a constant ion to carbon atom arrival ratio. Film composition and density were determined by ion scattering techniques (RBS and ERDA), indicating a negligible hydrogen content and a density dependence with the assistance voltage. The bonding structure of the films has been studied by Raman and X-ray Absorption Near-Edge (XANES) spectroscopy. Different qualitative effects have been found depending on the ion energy range. For ion energies below 300 eV, there is a densification of the carbon layer due to the increase in the $sp^3$ content. For ion energies above 300 eV sputtering phenomena dominate over densification, and thinner films are found with increasing assistance voltage until no film is grown over 600 V. The films with the highest $sp^3$ content are grown with intermediate energies between 200-300 V.

## 1. INTRODUCTION

Amorphous carbon (a-C) has been the object of intense research in the last decades because of its unique properties and applications. The properties of this material are controlled by the bonding structure which is mainly defined by the $sp^3/sp^2$ ratio and by the hydrogen content [1]. Normally, amorphous carbon films are grown with a high $sp^2$ content since this is the most stable hybridisation. The increase in the number of $sp^3$ bonds in the film can be achieved if carbon particles with energies in the 10-1000 eV range reach the surface. Normally, this is attained with growth methods involving positive ion bombardment ($C^+$, $CH_4^+$, ...) permitting a fine control of the arrival ion energy.

The high $sp^3$ content gives this material diamond-like (DLC) properties such a high hardness, infrared transparency and chemical inertness [2]. However, films with a high concentration of $sp^3$ bonds present great values of internal stress which makes the films mechanically unstable, and limits the thickness that can be grown [3]. The incorporation of hydrogen to the structure of the films increases the stability by providing stress relief but decreases the mechanical performances of the films, which become more polymeric [4].

For these reasons, novel techniques are being developed with the aim of producing stable carbon films with high $sp^3$ contents and without the presence of hydrogen in the structure. Ion beam assisted deposition (IBAD) of evaporated or sputtered graphite is a promising technique for growing films without any hydrogen content. The energy of the carbon atoms is about 0.1 eV and 10 eV for evaporation and sputtering, respectively, which produces basically $sp^2$ bonded films [5]. With the ion assistance, one can increase the arrival energy of the carbon atoms at the substrate and, hence, the $sp^3/sp^2$ ratio. The IBAD technique allows the design of the film properties by controlling independently the ion to carbon arrival ratio and the ion energy. In this present work we report a study of the effect of the energy of concurrent $Ar^+$ ions on evaporated carbon films.

## 2. EXPERIMENT

Amorphous carbon films were grown in a high vacuum chamber with a base pressure of $2x10^{-7}$ mbar on p-type (100) oriented Si substrates. Before entering the chamber, the substrates were successively in trichloroethylane, acetone and ethanol. An electron gun was used to evaporate graphite lumps of approximately 3 mm size. The evaporation rate was kept constant at a value of ~2 Å/s by controlling the electron beam current and monitoring the thickness with a quartz crystal microbalance located near the substrate. The electron beam current used to evaporate the graphite target was varied between 90-120 mA and the electrons were accelerated at a voltage of 7 kV. The assistance process was performed with a concurrent $Ar^+$ ion bombardment during the evaporation time using a 3 cm beam diameter Kauffman-type ion gun. The total ion current was 10 mA and the acceleration voltage was varied between 100-800 V. The ion current was non-neutralised in order to open the beam and cover a broader area. This favours the production of homogeneous films in the substrate. During

## DISCLAIMER

deposition the substrates were held at a temperature of 100°C.

The angle of ion assistance, i.e. the angle between the ion beam and the substrate normal, was fixed to 50°, as close as possible within the experimental constraints to the optimal value of 60° found in carbon films [6]. This is an important parameter in ion assisted deposition techniques since the sputtering yield and ion penetration depth depend strongly on it. Oblique incidence reduces the penetration depth of the ions, increasing the bombardment effects in the near surface region. For $Ar^+$ bombardment of carbon, the sputtering yield follows a $\cos^{-1}\theta$ law, increasing smoothly from normal incidence, $\theta = 0°$, and reaching a maximum around 60° [7].

The film thickness was measured with a Dektak 2020 profiling system. The composition and density of the films were estimated by Rutherford Backscattering Spectrometry (RBS) and Elastic Recoil Detection Analysis (ERDA) techniques. The experiments were carried out with the tandem accelerator facility at Sandia National Laboratories. RBS was performed with 3.73 MeV $^4He$ and 164° scattering angle. At this energy, the scattering cross section for the carbon is non Rutherford, with a signal enhanced by about seven times the Rutherford value [8,9]. ERDA measurements were performed with 26 MeV $^{28}Si$ ions and a range foil of Mylar 12μm thick. The incident angle in the scattering geometry was 75° and the exiting angle 75°, leading to a scattering angle of 30°. With this configuration carbon and hydrogen are well detected giving non overlapping signals. The oxygen present in the film is also detected, although the signal partially appears in the low energy side of the spectrum. The quantification of the RBS and ERDA spectra was done with the computer code SIMNRA [10]. This code allows for the simulation of these spectra using Rutherford scattering cross section values, as well as non Rutherford cross section values using tabulated data existing in the literature.

Raman spectroscopy was used to study the bonding nature of the amorphous carbon films. The spectra were obtained with a DILOR x-y microRaman system using the 514 nm line of an Ar laser. In Raman spectroscopy of carbon films, the efficiency for $sp^2$ bonds is about 50 times that of $sp^3$ [11]. This drawback makes it difficult to quantify the $sp^2/sp^3$ content, although it has been found a good correlation between Raman spectra and film properties [12].

More detailed information on the bonding structure was obtained with x-ray near edge absorption spectroscopy (XANES), a technique particularly sensitive to the bonding environment which provides very different signals for graphite and diamond with the advantage of a similar cross section, and works well even in amorphous and nanocrystalline systems [13]. The XANES experiments were performed at the beamline 8.2 of the Stanford Synchrotron Radiation Laboratory (SSRL). The data were collected in the total yield mode by recording the sample current to ground, and were normalised to the signal coming from a gold-covered grid located upstream in the x-ray path. The angle between the sample normal and the incident light was near 55° to avoid preferential bond orientation effects.

## 3. RESULTS AND DISCUSSION

### a) Profilometry

By profilometry we have determined the film thickness. Fig. 1 shows the thickness from a set of samples grown with different assistance voltages. The thickness was measured at several different points within each sample and is represented by the average value. All the measurements were within the error bars indicating a good homogeneity in the film thickness. A general trend in Fig. 1 is the decrease of the film thickness with increasing assistance voltage. Qualitatively, we can differentiate three regions. In region I there is a slight decrease in the thickness as we increase gradually the assistance voltage. For energies in the range of region II, a sharper change is found and the thickness decreases drastically until, in region III, no films is obtained.

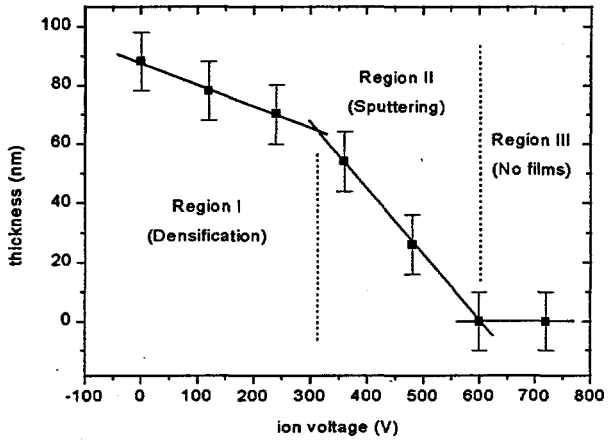


**Figure 1.** Thickness of a set of films grown with different assisting ion voltages. Three regions can be distinguished according to the qualitative effects of the ion assistance.

Taking into account that the flux of carbon atoms reaching the substrate is kept constant for the whole assistance voltage range, the decrease in the film thickness can be explained by two different factors. Firstly, the $Ar^+$ ions can transfer energy to the impinging carbon atoms via elastic atomic collisions, producing energetic bonding configurations (like $sp^3$ hybridisation or bonding structures with interstitial atoms) that yield carbon films denser than graphite. Secondly, the $Ar^+$ ions produce sputtering of carbon with loss of matter in the film [14]. From Fig. 1, it is clear that the dominant process in the region II is sputtering. However, it is not clear if the thickness decrease in region I is due to a slight sputtering or to densification. This question can be directly answered by determining the film density as is described below.

### b) RBS and ERDA

The techniques RBS, detecting C, N, O and Ar, and ERDA, detecting C, H and O, give complementary information of the film composition. Also, they provide an estimation of the accuracy of the compositional analysis based on the amount of carbon provided by each technique. The two types of measurement were made in different sessions, one at a time. Fig. 2 shows the RBS spectrum of

the sample grown with an assistance voltage of 120 eV. The experimental curve is represented with open dots, and the spectrum simulated using the SIMNRA code, with a continuous line. The enhancement of the C signal due to the non Rutherford cross section value is evident.

Fig. 3 shows the ERDA spectrum for the same sample (120V). As in the RBS spectra, the open dots represent the experimental spectrum and the continuous line the simulated spectrum. For the simulations of the RBS and ERDA spectra, the same sample composition has been assumed. This procedure has been applied to all the samples analysed.

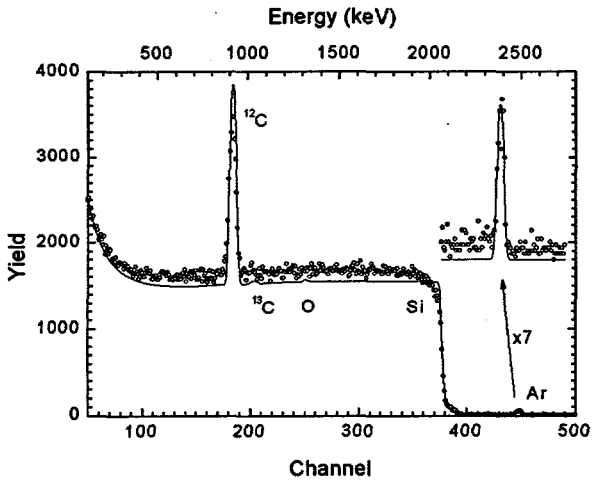


**Figure 2.** RBS spectrum of the sample grown with assistance of 120 eV $Ar^+$ ions. Due to the energy of the incident He ions, 3.73 MeV, the C is about 7 times higher than the Rutherford value. The experimental spectrum is shown in open dots and the continuous line represents the simulation.

Table 1 contains the results from the ion beam analysis. From the compositional analysis it can be pointed out that the films are mainly composed by carbon with a small amount of argon, oxygen and hydrogen. The amount of argon in the samples is quite small with respect to carbon and its value increases with the applied acceleration voltage until a saturation percentage of 3% is reached. The results for the thinner film (480V) are not indicated because there is a great uncertainty in the fitting procedure and the error in the thickness (around 50%) give useless values.

**Table 1.** Composition and density results from the ion beam analysis of the samples shown in Fig. 1.

| Assistance voltage (V) | %C | %Ar | %O | %H | d (g/cm$^3$) |
|---|---|---|---|---|---|
| 0 | 98 | 0 | 1 | 1 | 2.1 ± 0.2 |
| 120 | 96 | 1 | 2 | 1 | 2.3 ± 0.2 |
| 240 | 94 | 3 | 2 | 1 | 2.5 ± 0.2 |
| 360 | 95 | 3 | 1 | 1 | 2.3 ± 0.2 |

The RBS and ERDA analysis provides also a value of the surface density of atoms. This quantity, converted to mass and divided by the thickness, is just the density of material. The values obtained from this analysis are presented in Table 1, with an estimated error around 10%. These values show an increase in the density with the assistance voltage reaching a maximum for assistance with 240 eV ions, and a subsequent decrease for higher ion energies The density increase correlates well with the thickness decrease in the region I of Fig. 1, supporting the densification mechanism taking place for ion assistance in the 0-300 eV range. The next question is the nature of the structural changes leading to formation of denser films. Formation of amorphous carbon with a high $sp^3$ content can explain the increase in the density. Accordingly, the thinner and less dense films grown with high assistance voltage should correspond to a higher $sp^2$ content.

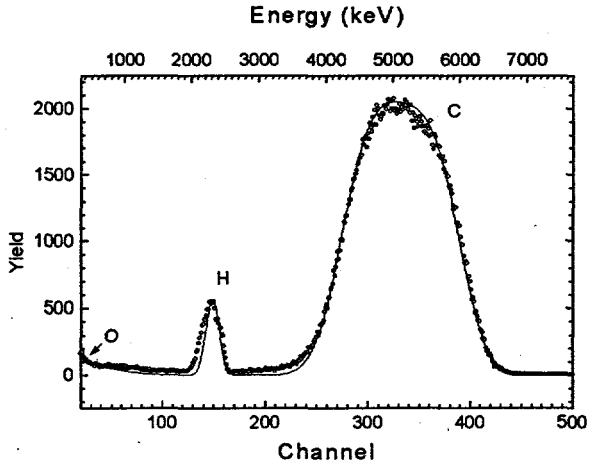


**Figure 3.** ERDA spectrum of the same sample considered in the RBS spectrum of Fig. 2.

**c) Raman spectroscopy**

Fig. 4 shows the Raman spectra, normalised to the same height, for the set of samples previously considered. The samples grown with 600 and 700 eV ion assistance yield only a noisy signal (not shown) due to the lack of appreciable film thickness. The experimental data have been fit with two gaussian distributions associated to the peaks commonly found in amorphous carbon and labelled as G (from graphite) at ~1580 cm$^{-1}$ and D (from disordered) at ~1400 cm$^{-1}$. The origin and position of these peaks is briefly discussed as follows. Crystalline graphite shows a sharp and intense Raman peak at 1580 cm$^{-1}$ due to in-plane vibrations, that broadens and shifts to lower values with decreasing crystallite size. Small crystallite size graphite shows also a peak at ~1350 cm$^{-1}$ due to phonons with non-zero wavevector. This D peak is selection rule prohibited in a perfect crystal, but becomes visible due to uncertainty in the wavevector when dealing with small size domains. In microcrystalline graphite, G and D peaks are present, with an intensity ratio proportional to the particle size [15]. Crystalline diamond shows a sharp Raman peak at 1332 cm$^{-1}$ that disappears when the size of the diamond crystallites becomes nanometric. For nanometric diamond, the typical G and D bands of graphite are present, even if other techniques like XANES or x-ray diffraction, detect the presence of diamond [13,16,17].

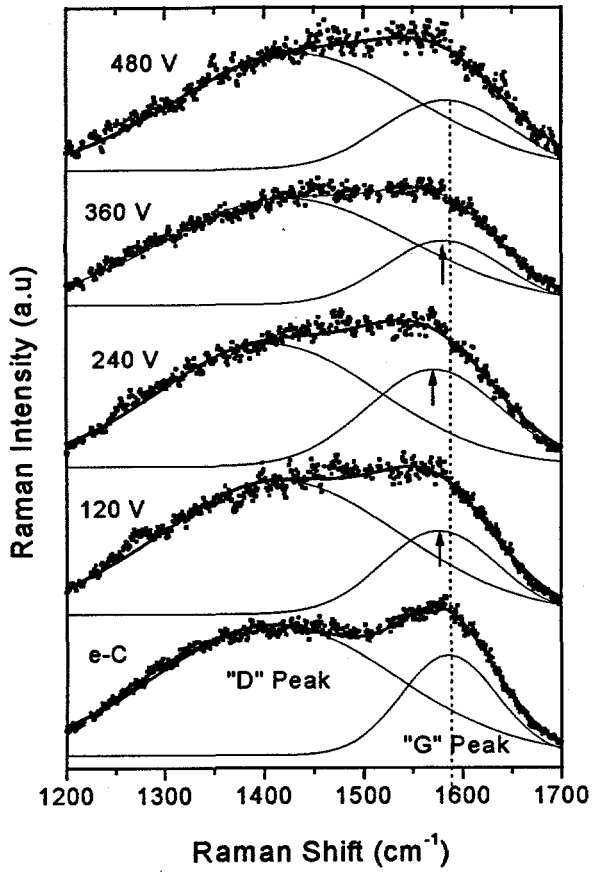


**Figure 4.** Raman spectra of the films considered in Fig. 1. The spectra have been fitted with two gaussian distributions labelled as G (graphite) and D (disordered). The shift of the Raman G peak, related to the $sp^3$ content, is clear in the figure.

Since Raman is a bulk technique (i.e. light can penetrate several microns in the solid, probing the whole thin film ), the Raman intensity is, in principle, proportional to the number of atoms in the film corrected by the cross section. If the cross section were a constant value, independent of the carbon hybridisation, then the Raman intensity normalised to the film thickness would be a measure of the density. However, the cross section for $sp^2$ bonded carbon is about 50 times that of $sp^3$ carbon, while the density of diamond is approximately twice that of graphite. Therefore, the carbon Raman intensity normalised to the thickness is essentially a measure of the proportion of $sp^2$ carbon atoms in the film

In Figure 5(a) is shown the overall intensity of the Raman signal in the carbon region normalised to film thickness taken from Fig. 1. A first observation is the significant decrease in the signal for the IBAD films compared to the evaporated film without assistance. This can be explained by the higher $sp^3$ content in the IBAD films. The intensity reaches a minimum at 240 V, in agreement with the maximum density value and with a maximum proportion of $sp^3$ bonded carbon. This result supports the densification mechanism taking place in region I of Fig. 1 as due to formation of tetrahedral bonding. For assistance voltages above 300 V the normalised Raman intensity increases, in agreement with the density and $sp^3$ content decrease.

Additional information on the bonding structure of the films can be obtained from the curve fitting of the Raman spectra. In Fig. 4 is evident an energy shift of the G component depending on the growth conditions. Previous work has found that the position of this peak depends on the bonding nature of the films and that, hence, it is another indication of the $sp^3$ content. Experimentally, it has been found that for non-hydrogenated films there is a shift towards lower frequencies as the number of $sp^3$ sites increases [18]. Even if this shift does not yield quantitative information on the $sp^3$ content, it is useful to qualitatively determine the best films from a diamond-like environment perspective. Figure 5(b) displays the position of the G peak for our films. A minimum is reached for the assistance voltage of 240 V, corresponding to the film with the highest $sp^3$ content, in agreement with the previous results.

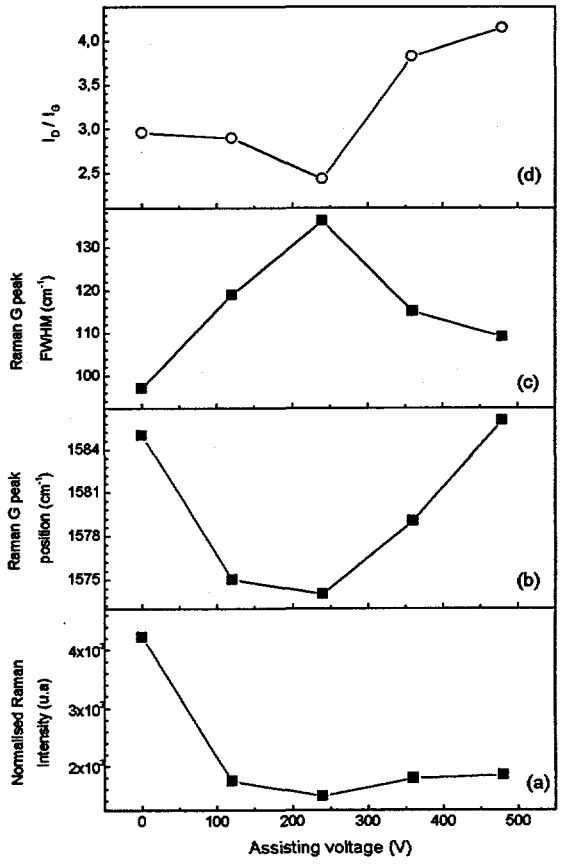


**Figure 5.** (a) Raman signal normalised to the film thickness for a set of films grown with different assistance voltages. Since the cross section for $sp^2$ bonded carbon is ~50 times that of $sp^3$ carbon, the minimum intensity corresponds to a maximum $sp^3$ content. (b) Position of the Raman G peak vs. assistance voltage. The minimum in the position of this peak indicates a maximum in the $sp^3$ content. (c) Full width at half maximum for the G peak vs. assistance voltage. (d) Intensity ratio of the "disordered" to "graphite" Raman peak.

Structural information can be also derived from the spectral shape of the Raman peaks. The full width at half maximum (FWHM) and relative intensity of the G peak provides information about the disorder and about the diamond-likeness of the films [19,20]. The FWHM value is

related with the bond angle distortion, varying from 3 $cm^{-1}$ in microcrystalline graphite to several hundreds in amorphous films. From Fig. 4 is clear that peak G broadens with increasing assistance voltage with values around 100 $cm^{-1}$. From Fig. 5(c) we can see that the maximum disorder corresponds with the maximum $sp^3$ content. In addition, the minimum of the $I_D/I_G$ ratio, as illustrated in Figure 5(d), indicates again that the best films are obtained for a voltage value around 240V.

In summary, all the information derived from the Raman spectra suggest that the densification of the films is due to formation of a significant number of $sp^3$ bonded sites. However, Raman cannot discern if the $sp^3$ bonding is segregated from the $sp^2$ domains or if a true amorphous network is formed. Also, quantification of the $sp^3$ content is beyond the possibilities of Raman spectroscopy in this system. A technique more sensitive to the local structure like XANES is, hence, used.

**d) XANES**

XANES spectroscopy has been used to quantify the $sp^3$ content, to obtain information on the homogeneity, and isotropy of the films, and to check its thermal stability. It is noteworthy that RBS found almost no hydrogen, hence all the features must correspond to the actual arrangement in an amorphous network of fourfold and threefold coordinated carbon.

Fig. 6 shows photoabsorption spectra at the C(1s) edge, normalised to the same height, for the whole set of films considered in this study together with graphite and diamond references of $sp^2$ and $sp^3$ bonding, respectively. The graphite spectrum shows an absorption threshold of transition to $\pi^*$ states at 284 eV and a second threshold of transitions to $\sigma^*$ states at 291 eV. Diamond lacks $\pi^*$ states and hence shows a single absorption edge at 289 eV.

The areal homogeneity of films was verified by repeating the measurements in the central and peripheral regions of each sample, an identical spectrum being obtained. This result is very interesting for technological applications since films deposited with other techniques, like filter cathodic vacuum arc (FCVA) and mass selected ion beam (MSIB), present homogeneity problems due to the use of magnetic filters which limit the coating area [2].

The overall shape of all the amorphous carbon spectra in Fig. 6 is rather similar, except for the sample grown with assistance of 600 eV ions. As shown in Fig.1, under those conditions no film is grown due to dominant sputtering processes. Since XANES is a surface technique with a probing depth determined by the ~50 Å escape depth of the low energy electrons, even the samples grown with 600 and 700 eV ion assistance where no film was detected, present carbon XANES intensity. The carbon signal in this case is dominated by C=O surface contamination on the silicon substrate, and serves as a reference. The rest of the samples present also a small peak at 288.5 eV due to C=O contamination, that does not mask the features due to the amorphous carbon film.

The films grown with 0-480 eV ion assistance show a $\pi^*$ peak, indicating the presence of $sp^2$ bonded carbon, although much broader than the graphite reference. The broadening seems related to the contribution from incomplete and disordered graphitic-like coordination of carbon atoms in the amorphous films. The spectra do not show separated $\sigma^*$ absorption edges related to $sp^2$ and $sp^3$ phases, hence indicating that mixing of threefold and fourfold coordinated carbon occurs at the atomic level, with the related absorption thresholds merging to form a smooth edge starting at 289 eV. These are the features commonly found in amorphous diamond-like carbon. [21, 22]

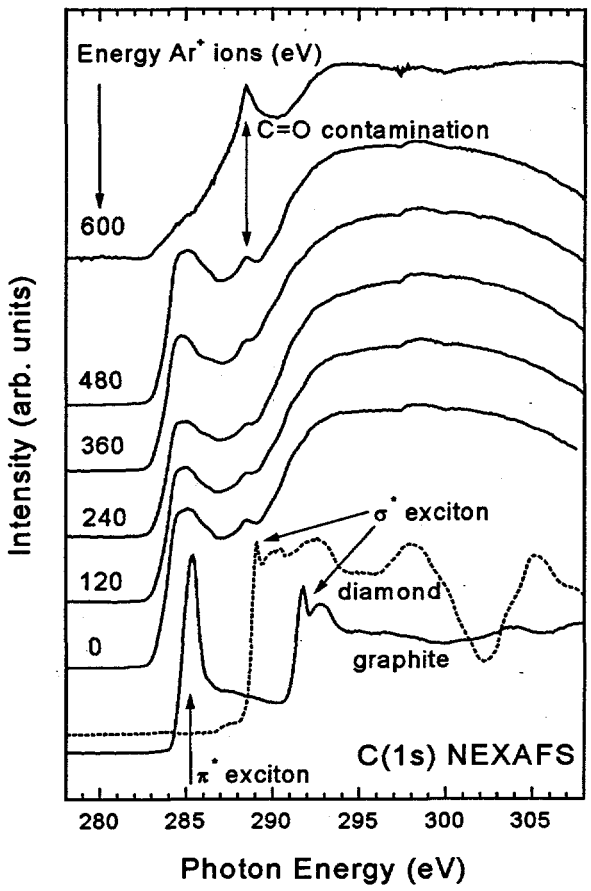


**Figure 6.** XANES C(1s) spectra of amorphous carbon films grown with different $Ar^+$ ion assistance energies, together with graphite and diamond references.

The quantification of the $sp^2/sp^3$ content in the films can be derived from the relative intensity ratio of $\pi^*/\sigma^*$ states. For computing purposes, the area below the spectra between 282 and 287 eV was assigned to $\pi^*$ states and the area between 284 and 301 eV to $\sigma^*$ states. The intensity ratios were compared with the spectrum from the sample grown without assistance, whose $sp^2$ content is considered 95% from comparison with previous work on similarly grown samples [2,23,24]. One should note that comparison with the intensity ratio from the graphite crystalline reference is not valid, since the $\pi^*$ peak has an excitonic origin as its intensity depends strongly on the microstructure which affects electron localisation [25]. In fact, the $\pi^*$ intensity of the film grown without ion assistance is 76% of that found in the graphite reference, a value too low to be assigned to the $sp^2$ content. The $\pi^*$ intensity ratio and the corresponding $sp^2$ content are displayed in Figure 7 for the

whole set of films. The dependence agrees well with the qualitative results from Raman and confirms that ion assistance with 240 eV produces a significant amount of $sp^3$ bonded atoms.

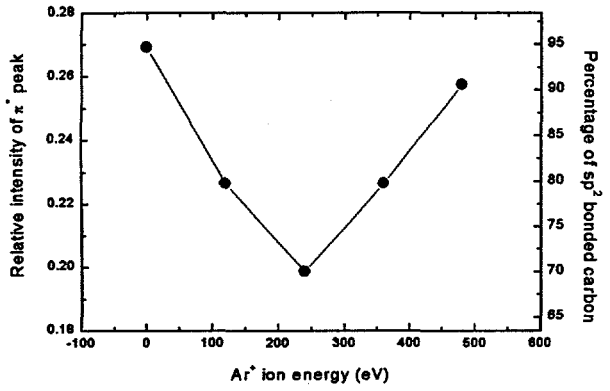


**Figure 7.** Relative intensity of the $\pi^*$ features in the XANES spectra of Fig. 6, related to the $sp^2$ content.

It is interesting to compare our results with previous reports on ion assisted growth techniques. When the carbon atoms are directly accelerated at a certain voltage, the maximum content of $sp^3$ bonds is found for values around 100 eV [26]. This deposition mechanism is generally described, as in c-BN, by a subplantation model [27,28]. This mechanism is based on incident energetic ions that penetrates into subsurface sites and provide a quenched-in increase in density and $sp^3$. In our case, the carbon atoms are accelerated by elastic collisions with Ar ions, the energy transfer depending on the scattering angle. In the case of C-Ar collision, by simple classical mechanics calculations the average energy transferred to the incident carbon atom is about one half of the initial Ar ion energy. Hence, our optimal ion energy is in agreement with direct acceleration results. In our case the lower $sp^3$ content (~30%) achieved, compared with other techniques like FCVA or MSIB, is explained by the broad distribution of energies as a consequence of the collision processes. Also, the ion to carbon arrival ratio could be optimised in order to increased the $sp^3$ content. The effect of this ratio in our deposition system is actually under study.

An angular dependent XANES study has been performed on several samples, to check if preferential orientation of $sp^2$ phases occurs in the films. Due to the linear polarisation of the synchrotron light, changes in the relative intensity of the $\pi^*$ states with the angle between the beam and the sample normal can be related to preferential orientation of the $sp^2$ phase [29]. The preferential orientation of basal planes in ion assisted deposition techniques is an important issue due to its connection to the attaining of separated $sp^3$ phases in diamond [30] and the isoelectronic material c-BN [31]. In this case, however, the spectra were identical for incidence angles between 0° (normal incidence) and 75° (glancing incidence), evidencing totally isotropic films.

We have also studied the thermal stability of the films, by performing successive cycles of annealing in vacuum and XANES measurements. The films were resistively annealed up to 550°C by direct flow of current through the Si substrate, the heating being maintained for one minute. The temperature was determined with an IRCOM infrared pyrometer with a threshold detection temperature of 350°C. Temperatures below this limit were estimated from calibration of the electric power applied to the samples. Fig. 8 contains the C(1s) spectra representing successive annealing cycles of increasing temperatures in one of the samples. A significant change in the $\pi^*$ signal occurs, the variation of the intensity ratio with temperature being plotted in the inset. The sample becomes more graphitic with annealing, the faster change taking place at 250°C, and slowing down at 450°C. This graphitization is a well known process which leads to the deterioration of the film quality due to the reduction of the $sp^3$ content for temperatures above 200°C [32,33] and a complete graphitization of the samples is normally obtained for temperatures above 500°C [34]. Therefore, our samples exhibit a similar temperature unstability as previous reports in equivalent films.

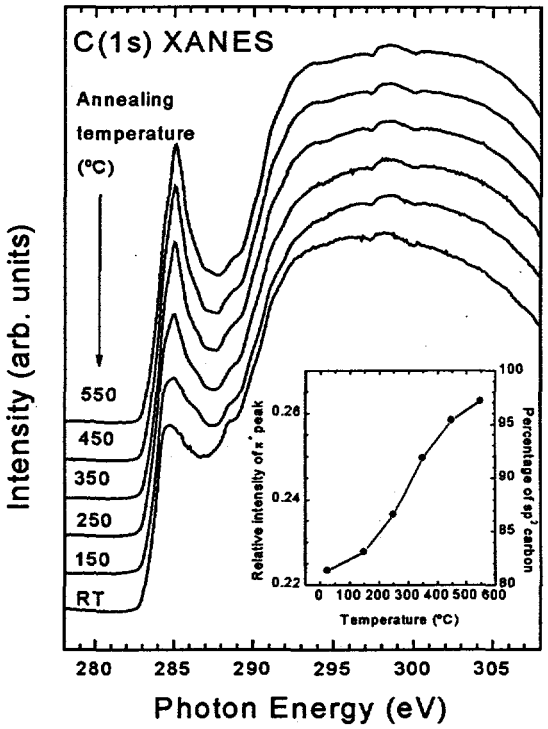


**Figure 8.** XANES spectra for annealed IBAD samples.

The increase of the $\pi^*$ signal upon annealing does not take place in the whole 283-287 eV region, but only at 285.4 eV, i.e. the energy of the $\pi^*$ excitonic peak in the graphite reference. Accordingly, the peak in the annealed samples appears sharper. This evidences the presence of several unresolved components in the $\pi^*$ region due to defective graphitic bonding, somehow resembling the observation of defective $\pi^*$ peaks in the isoelectronic material h-BN [35]. This point is actually under study.

## 4. CONCLUSIONS

The composition and bonding in amorphous carbon thin films grown by ion beam assisted deposition has been examined by combining profilometry, ion scattering (RBS and ERDA), Raman and XANES measurements. Raman and XANES are complementary techniques to study the structure of amorphous carbon films. Even if XANES provides a better quantification of the $sp^2/sp^3$ content, a combination of profilometry and Raman intensity and lineshape studies provides a good estimation.

Amorphous carbon films with a significant $sp^3$ content can be grown using $Ar^+$ assistance. The films are dense and contain almost no hydrogen. The optimal ion assistance energy is ~250 eV. Since the carbon atoms are accelerated by elastic collisions with the Ar ions, this value corresponds to an average carbon energy of ~100 eV. Energy transfer by collisions with assisting ions opens the path to the use of reactive assisting ions.

The films grown by ion beam assisted deposition are amorphous, isotropic, very homogeneous, and are thermally unstable above ~200°C.

## ACKNOWLEDGMENTS

This work has been partially financed by the Spanish CICYT under projects MAT96-0529-C02-01 and PB971224, the CAM project no. AE 00140/94, the NATO project CRG-971539, and the US Department of Energy through Lawrence Livermore National Laboratory under contract W-7405-ENG-48. The work was performed at the Stanford Synchrotron Radiation Laboratory, which is supported by the DOE, Office of Basic Energy Science. The grant AP96 from the F.P.U. program of the Spanish M.E.C. is also appreciated.



## REFERENCES

1. J. Robertson, Current Opinion in Solid State and Mat. Sci. **1** (1996) 557.
2. J. Robertson, Adv. Phys. **35** (1986) 317.
3. J.C. Angus, C.C. Hayman. Science **241** (1988) 913.
4. J.C. Angus, F. Jansen, J. Vac. Sci. Technol. A **6** (3) (1988) 1778.
5. J. Robertson, E.P. O'Reilly. Phys. Rev. B **35** 6 (1987) 2946.
6. J.Ullmann, U.Falke, W.Scharff, A.Schröer, G.K.Wolf. Thin Solid Films **232** (1993) 154.
7. J.J. Cuomo, S.M. Rossnagel, H.R. Kauffman. 'Handbook of ion beam processing technology' Noyes Publications (1989) 80.
8. Y. Feng, Z. Zhou, Y. Zhou, and G. Zhou. Nucl. Instrum. Methods B **94** (1994) 11
9. J.A. Leavitt, L.C. McIntyre Jr., P. Stoss, J.G. Oder, M.D. Ashbaugh, B. Dezfouly-Arjomandy, Z.M. Yang and Z. Lin, Nucl. Instrum. Methods B **40/41** (1989) 776
10. M. Mayer, SIMNRA User's Guide v.4.0, Max-Plank-Institute für Plasmaphysik, 1997/98
11. Bou P. and Vandenbulcke. J. Electrochem. Soc. **138** (10) (1991) 2991.
12. Tamor M.A., Vassell W.C. J. Appl. Phys. **50** (1994) 3823.
13. M. M. Garcia, I. Jiménez, L. Vázquez, C. Gómez-Aleixandre, J. M. Albella, O. Sánchez, L. J. Terminello, and F. J. Himpsel, Appl. Phys. Lett. **72** (1998) 2105.
14. W. T. Zheng, E. Broitman, N. Hellgren, K.Z. Xing, I. Ivanov, H. Sjöström, L. Hultman, and J. E. Sundgren, Thin Solid Films **308-9** (1997) 223.
15. F. Tuinstra and J.L. Koenig, J. Chem. Phys. **53** (3) (1970) 1126.
16. F. L. Coffman, R. Cao, P. A. Pianetta, S. Kapoor, M. Kelly, and L. J. Terminello, Appl. Phys. Lett. **69** (1996) 568.
17. D. M. Gruen, A. R. Krauss, and C. D. Zuiker, R. Csencsits, L. J. Terminello, J. A. Carlisle, I. Jiménez, D. G. J. Sutherland, D. K. Shuh, W. Tong, and F. J. Himpsel, Appl. Phys. Lett. **68** (1996) 1640.
18. S. Prawer, K.W. Nugent, Y. Lifshitz, G.D. Lempert, E.Grossman, J. Kulik, I. Avigal, R. Kalish. Diam. and Rel. Mat. **5** (1996) 433.
19. R.O.Dillon, J.A.Woollam, Phys. Rev. B **29** (6) (1984) 3482.
20. H.J. Scheibe, D. Drescher, P. Alers, Fres. J. of Anal. Chem. **353** (1995) 695.
21. J. Fink, T. Müller_Heizerling, J. Plüger, A. Bubenzer, P. Koidl, G. Crecelius, Solid State Commun. **47** 687 (1983).
22. L. Fayette, B. Marcus, M. Mermoux, G. Tourillon, K. Laffon, P. Parent, and F. LeNormand, Phys. Rev. B **57** (1998) 14123.
23. J. Robertson, Diam. and Relat. Mater. **1** (1992) 397.
24 E. Grossman, G. D. Lempert, J. Kulik, D. Marton, J. W. Rabalais, and Y. Lifshitz, Appl. Phys. Lett. **68** (1996) 1214.
25. J. Díaz, S. Anders, X. Zhou, E. J. Moler, S. A. Kellar, and Z. Hussain (unpublished).
26. P.F. Fallon, V.S. Veerasamy, C.A. Davis, J. Robertson, G.A.J. Amaratunga, W.I. Milne, J. Koskinen, Phys. Rev. B **48** (7) (1993) 4777.
27. Y. Lifshitz, S.R. Kasi, and J.W. Rabalais, Phys. Rev. B **41** (15) (1990) 10468
28. J. Robertson, Diam. and Rel. Mat. **3** (1994) 361
29. R. A. Rosenberg, P. J. Love, and V. Rehn, Phys. Rev. B **33** (1986) 4034.
30. I. Jiménez, M. M. García, J. M. Albella and L. J. Terminello, Appl. Phys. Lett. (in press) 16 Nov. 1998.
31. D. J. Kesker, D. S. Ailey, and R. F. Davis, J. Mater. Res., **8** (1993) 1214.
32. R. Gago, O. Sánchez, A. Climent-Font, J.M. Albella, E. Román, E. Raühala, J. Raisänen, Thin Solid Films (in press).
33. M. Chhowalla, J.Robertson, C.W.Chen, S.R.P.Silva, C.A.Davis, G.A.J.Amaratunga, W.I.Milne. J. Appl. Phys. **81** (1) (1997) 139.
34. D.R.Tallant, J.E. Parmeter, M.P.Siegal, R.L.Simpson. Diam. and Rel. Mat. **4** (1995) 191.
35. I. Jiménez, A. F. Jankowski, L. J. Terminello, J. A. Carlisle, D. G. J. Sutherland, G. L. Doll, W. M. Tong, D. K. Shuh, and F. J. Himpsel, Phys. Rev. B **55** (1997) 12025.

X-Sender: aclimfon@bosque.sdi.uam.es
Date: Wed, 28 Oct 1998 15:20:56 +0200
To: "Barney L. Doyle" <bldoyle@sandia.gov>
From: Aurelio Climent-Font <acf@uam.es>
Subject: Hello!

P ——> sign off.

Hi Barney!

It has been a long time since we were in touch for the last time. As you can imagine I am very busy with my teaching (I have all the teaching of the year concentrated in this semester) and having meetings about the accelerator project. For this project there is a comission of 6 people (I am a member of it).

Two weeks ago we had in Madrid a three day meeting with George Amsel, from 9 in the morning until 9 in the evening. After that, the last day we were really exhausted, we concluded that the most convenient machine to buy in view of the research program discussed would be a 4 MV tandem. We made a list of minimum requisits to be fulfilled by the machine that we have already sent to NEC and HVEE. So, to decide where we will buy, NEC or HVEE, may still take some time.

With the RBS and ERD measuraments I made on C films from Spain we have written a paper including results ~~on XANES and IR spectroscopy~~. The paper has just been submitted ~~in~~ Diamond and Related Materials, I send you with this e-mail a copy of it (attached file ibaddlcl.doc).

Jammd

As we discussed ~~some time before I left~~ Sandia, I have in mind submitting a paper on TOF at the next IBA conference in Dresden, although so far I have not worked too much on it. By the end of January I will concentrate on this work.

Please say hello to everybody in the lab.

Best regards,

Aurelio

%%%%%%%%%%%%%%%%%%%%%%%%%%
Aurelio Climent-Font
Departamentro de Física Aplicada
Universidad Autónoma de Madrid
Cantoblanco, E-28049 Madrid, Spain
Phone: +34 91 397 5264
Fax: +34 91 397 3969
e-mail: acf@uam.es
%%%%%%%%%%%%%%%%%%%%%%%%%%

ibaddlc1.doc

%%%%%%%%%%%%%%%%%%%%%%%%%%
Aurelio CLIMENT-FONT
Departamentro de Física Aplicada
Universidad Autónoma de Madrid
Cantoblanco, E-28049 Madrid, Spain
Phone: +34 91 397 5264
Fax: +34 91 397 3969
e-mail: acf@uam.es
%%%%%%%%%%%%%%%%%%%%%%%%%%